Fast Rotation of a Bose-Einstein Condensate

Vincent Bretin, Sabine Stock, Yannick Seurin, and Jean Dalibard
Laboratoire Kastler Brossel, * 24 rue Lhomond, 75005 Paris, France*
(Received 18 July 2003; published 4 February 2004)

We study the rotation of a ^{87}Rb Bose-Einstein condensate confined in a quadratic plus quartic potential. This trap configuration allows one to increase the rotation frequency of the gas above the trap frequency. In such a fast rotation regime we observe a dramatic change in the appearance of the quantum gas. The vortices which were easily detectable for a slower rotation become much less visible, and their surface density is well below the value expected for this rotation frequency domain. We discuss some possible tracks to account for this effect.

DOI: 10.1103/PhysRevLett.92.050403 PACS numbers: 03.75.Lm, 32.80.Lg

The fast rotation of a macroscopic quantum object often involves a dramatic change of its properties. For rotating liquid ^{4}He, superfluidity is expected to disappear for large rotation frequencies [1]. A similar effect occurs for type-II superconductors placed in a magnetic field, which lose their superconductivity when the field exceeds a critical value [2]. For the last few years it has been possible to set gaseous Bose-Einstein condensates into rotation, by nucleating in the gas quantized vortices which arrange themselves in a triangular lattice [3–7]. The theoretical investigation of these fast rotating gases has led to several possible scenarios depending on the confinement of the gas: nucleation of multiply charged vortices [8–14], melting of the vortex lattice [15], or effects closely connected to quantum hall physics [16–20].

Consider a condensate transversely confined by a harmonic potential with frequency $\omega_\perp$. For an angular momentum per particle $L_z \gg \hbar$, the condensate contains many vortices [21] and the coarse grained average of the velocity field is identical to that of a rigid body with angular frequency Ω [1]. The limiting case $\Omega = \omega_\perp$ corresponds to $L_z = \infty$ and is thus singular. This can be understood in the frame rotating at frequency Ω, where the trapping force is compensated by the centrifugal force and only the Coriolis force remains. The physics of this situation is analogous to that of charged particles in a uniform magnetic field and one expects to recover for weak interactions an energy spectrum with Landau levels separated by $2\hbar\omega_\perp$. However the absence of confinement in a harmonic trap rotating at $\Omega = \omega_\perp$ makes this study experimentally delicate [22]. The Boulder group recently reached $\Omega = 0.99\omega_\perp$ using evaporative spin-up [23].

In the present paper, following suggestions in [8–11] we study the rotation of a Bose-Einstein condensate in a trap whose potential is well approximated by a superposition of a quadratic and a small quartic potential:

$$V(\boldsymbol{r}) \simeq \frac{1}{2}m\omega_z^2 z^2 + \frac{1}{2}m\omega_\perp^2 r_\perp^2 + \frac{1}{4}k r_\perp^4 \qquad (k > 0), \quad (1)$$

where $x^2 + y^2 = r_\perp^2$. We can thus explore with no restriction the domain of rotation frequencies Ω around $\omega_\perp$. For $\Omega/\omega_\perp < 0.95$ we observe a regular vortex lattice. This lattice gets disordered when Ω increases. For $\Omega > \omega_\perp$ the number of detectable vortices is dramatically reduced although we have clear evidence that the gas is still ultracold and in fast rotation. We conclude by proposing some possible explanations for this behavior.

Our ^{87}Rb condensate is formed by radio-frequency evaporation in a combined magnetic + laser trap. The pure magnetic trap provides a harmonic confinement along the three directions with the frequencies $\omega_\perp^{(0)}/2\pi = 75.5$ Hz and $\omega_z/2\pi = 11.0$ Hz. We superimpose a blue detuned laser (wavelength 532 nm) propagating along the z direction to provide the quartic term in the confinement. The potential created by the laser is

$$U(r_\perp) = U_0 \exp\left(-\frac{2r_\perp^2}{w^2}\right) \simeq U_0 - \frac{2U_0}{w^2}r_\perp^2 + \frac{2U_0}{w^4}r_\perp^4. \quad (2)$$

The laser's waist is $w = 25\ \mu$m and its power is 1.2 mW. The first term U_0 ($\sim k_B \times 90$ nK) on the right-hand side of (2) is a mere shift of the energy scale. The second term is a correction of the transverse trapping frequency; from the oscillation frequency of the center of mass of the condensate, we infer for the combined magnetic-laser trap $\omega_\perp/2\pi = 64.8(3)$ Hz [24]. The last term in (2) corresponds to the desired quartic confinement, with $k = 2.6(3) \times 10^{-11}$ J m^{-4}.

We start the experimental sequence with a quasipure condensate that we stir using an additional laser beam, also propagating along z [4]. This laser stirrer creates an anisotropic potential in the xy plane which rotates at a frequency $\Omega_{\rm stir}$. To bring the condensate in rotation at a frequency close to $\omega_\perp$, we use two stirring phases. First we choose $\Omega_{\rm stir}^{(1)} \simeq \omega_\perp/\sqrt{2}$, so that the stirring laser resonantly excites the transverse quadrupole mode $m = +2$ of the condensate at rest [25]. The duration of this first excitation is 300 ms and we then let the condensate relax for 400 ms in the axisymmetric trap. This procedure sets the condensate in rotation, with a vortex lattice containing typically 15 vortices.

We then apply the laser stirrer for a second time period, now at a rotation frequency $\Omega_{\rm stir}^{(2)}$ close to or even above

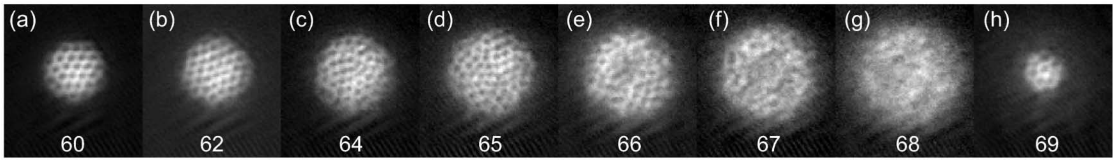

FIG. 1. Pictures of the rotating gas taken along the rotation axis after 18 ms time of flight. We indicate in each picture the stirring frequency $\Omega_{\rm stir}^{(2)}$ during the second stirring phase ($\omega_\perp/2\pi = 64.8$ Hz). The vertical size of each image is 306 μm.

$\omega_\perp$. For the condensate with 15 vortices prepared during the first phase, the transverse quadrupole mode is shifted to a higher frequency and can now be resonantly excited by a stirrer rotating at $\Omega_{\rm stir}^{(2)} \sim \omega_\perp$ [7,26]. The second stirring phase lasts for 600 ms. It is followed by a 500 ms period during which we let the condensate equilibrate again in the axisymmetric trap. At this stage the number of trapped atoms is 3×10^5.

We find that this double nucleation procedure is a reliable way to produce large vortex arrays and to reach effective rotation frequencies $\Omega_{\rm eff}$ around or above $\omega_\perp$. It has one drawback however: the effective rotation frequency $\Omega_{\rm eff}$ of the gas after equilibration might differ significantly from the rotation frequency $\Omega_{\rm stir}^{(2)}$ that we apply during the second stirring phase. The stirring phase injects angular momentum in the system, and the rotation frequency of the atom cloud may subsequently change if the atom distribution (hence the moment of inertia) evolves during the final equilibration phase.

The rotating atom cloud is then probed destructively by switching off the confining potential, letting the cloud expand during $\tau = 18$ ms and performing absorption imaging. We take simultaneously two images of the atom cloud after time of flight (TOF). One imaging beam is parallel to the rotation axis z and the other one is perpendicular to z [27]. Figures 1(a)–1(h) show images taken along the z axis and obtained for various $\Omega_{\rm stir}^{(2)}$ around $\omega_\perp$. When $\Omega_{\rm stir}^{(2)}$ increases, the increasing centrifugal potential weakens the transverse confinement. This leads to an increasing radius in the xy plane. As can be seen from the transverse and longitudinal density profiles of Fig. 2, obtained for $\Omega_{\rm stir}^{(2)}/2\pi = 66$ Hz, the gas after TOF has the shape of a flat pancake. The limit of our method for setting the gas in fast rotation is shown in Fig. 1(h). It corresponds to $\Omega_{\rm stir}^{(2)}/2\pi = 69$ Hz, far from the quadrupole resonance of the condensate after the first nucleation. In this case we could not bring the gas in the desired fast rotation regime.

For Figs. 1(e) and 1(f) obtained with $\Omega_{\rm stir}^{(2)}/2\pi = 66$ and 67 Hz, the optical thickness of the cloud has a local minimum in the center; this indicates that the confining potential in the rotating frame, $V_{\rm rot}(\boldsymbol{r}) = V(\boldsymbol{r}) - m\Omega_{\rm eff}^2 r_\perp^2/2$, has a Mexican hat shape. The effective rotation frequency $\Omega_{\rm eff}$ thus exceeds $\omega_\perp$. The striking feature of these images is the small number of visible vortices which seems to conflict with a large value of $\Omega_{\rm eff}$. The main goal of the remaining part of this Letter is to provide more information on this puzzling regime.

In order to analyze quantitatively the pictures of Fig. 1, we need to model the evolution of the cloud during TOF. For a pure harmonic potential ($k = 0$), a generalization of the analysis of [28] to the case of a rotating condensate shows that the expansion in the xy plane is well described by a scaling of the initial distribution by the factor $(1 + \omega_\perp^2\tau^2)^{1/2}$ [29,30]. We assume here that this is still approximately the case for a condensate prepared in a trap with a nonzero quartic term $kr_\perp^4/4$.

We have analyzed 60 images such as those of Fig. 1, assuming an initial Thomas-Fermi distribution:

$$n(\boldsymbol{r}) = \frac{m}{4\pi\hbar^2 a}[\mu - V_{\rm rot}(\mathbf{r})], \quad (3)$$

where $a = 5.2$ nm is the scattering length characterizing the atomic interactions and μ the chemical potential. The optical thickness for the imaging beam propagating along z, proportional to the column atomic density in the xy plane, varies as $(\alpha + \beta r_\perp^2 + \gamma r_\perp^4)^{3/2}$, where α, β, and γ can be expressed in terms of the physical parameters of the problem [31]. An example of the fit, which takes μ and $\Omega_{\rm eff}$ as adjustable parameters, is given in Fig. 2(a). The agreement is correct, though not as good as for condensates confined in purely harmonic traps. This may be a consequence of the approximate character of the scaling transform that we use to describe the TOF evolution. The resulting values for $\Omega_{\rm eff}$ as a function of $\Omega_{\rm stir}^{(2)}$ are given in Fig. 3. We find $\Omega_{\rm eff} \simeq \Omega_{\rm stir}^{(2)}$ for stirring frequencies ≤ 68 Hz. Note that for $\Omega_{\rm stir}^{(2)}/2\pi = 68$ Hz [Fig. 1(g)] the

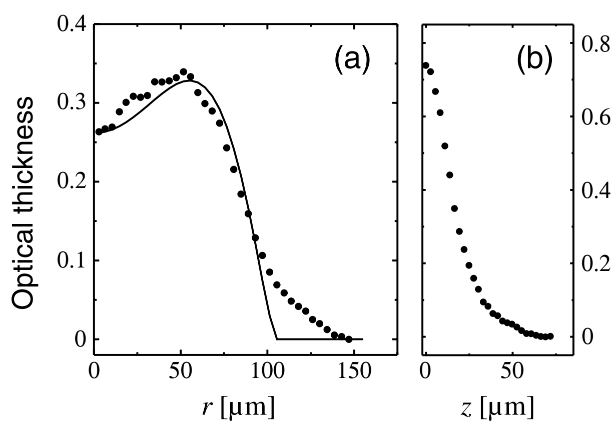

FIG. 2. Optical thickness of the atom cloud after time of flight for $\Omega_{\rm stir}^{(2)}/2\pi = 66$ Hz. (a) Radial distribution in the xy plane of Fig. 1(e). Continuous line: fit using the Thomas-Fermi distribution (3). (b) Distribution along the z axis averaged over $|x| < 20$ μm (imaging beam propagating along y).

quality of the fit is comparatively poor due to local inhomogeneities of the atom cloud.

From the value of μ given by the fit, we recover the atom number [8]. For $\Omega/(2\pi) = 67$ Hz, the Thomas-Fermi distribution (3) corresponds to a nearly spherical atom cloud before TOF (diameter 30 μm in the xy plane and length 34 μm along z).

A second determination of the effective rotation frequency $\Omega_{\rm eff}$ of the condensate is provided by the vortex surface density after TOF. This is measured manually by counting the number of vortices in a test surface of a given area (typically 25% of the whole area of the condensate). Assuming that the vortex pattern is scaled by the same factor as the condensate density, we deduce the vortex density n_v before TOF, hence the rotation frequency $\Omega_{\rm eff} = \pi\hbar n_v/m$ [21]. For $\Omega_{\rm stir}^{(2)} < \omega_\perp$, the value of $\Omega_{\rm eff}$ deduced in this way and plotted in Fig. 3 is in fair agreement with the one deduced from the fit of the images [32]. On the contrary, for $\Omega_{\rm stir}^{(2)}/2\pi = 66$–68 Hz the number of distinguishable vortices is much too low to account for the rotation frequencies determined from the fits of the TOF images. Further, in this regime no vortex lines are detectable in the images taken perpendicular to the z axis (not shown here), contrary to what happens for lower stirring frequencies [27,33].

In order to gather more information on the rotational properties of the gas, we now study the two transverse quadrupole modes $m = \pm 2$ of the gas. We recall that these two modes have the same frequency for a nonrotating gas, due to symmetry. For a rotating gas in the hydrodynamic regime, the frequency difference $\omega_{+2} - \omega_{-2}$ is proportional to the ratio between the average angular momentum of the gas and its moment of inertia, which is nothing but the desired effective rotation frequency $\Omega_{\rm eff}$ [26]. The strength of this approach is that it does not make any assumption on the expansion during TOF.

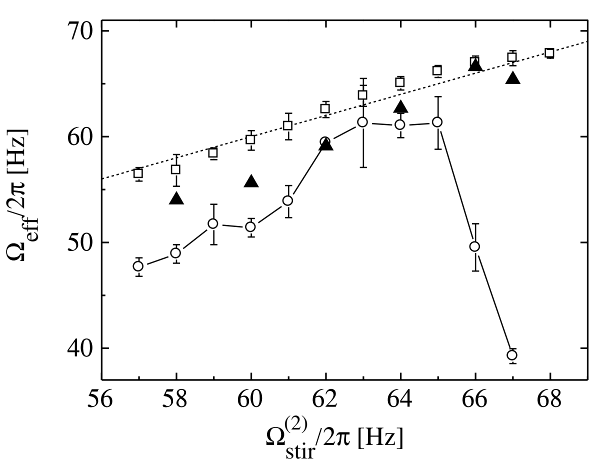

FIG. 3. Effective rotation frequency $\Omega_{\rm eff}$ as a function of the stirring frequency $\Omega_{\rm stir}^{(2)}$. □: values deduced from the fit using the Thomas-Fermi distribution (3). ○: values obtained by measuring the vortex density in the TOF pictures. ▲: values obtained using surface wave spectroscopy. The bars indicate standard deviations.

To study these quadrupole modes, we briefly illuminate the rotating gas using the laser stirrer, now with fixed axes [34]. This excites a superposition of the modes $m = \pm 2$ with equal amplitudes. We then let the cloud evolve freely in the trap for an adjustable duration and perform the TOF analysis. From the time variation of both the ellipticity of the cloud in the xy plane and the inclination of its eigenaxes, we deduce $\omega_{\pm 2}$, hence the effective rotation frequency $\Omega_{\rm eff} = (\omega_{+2} - \omega_{-2})/2$. The corresponding results are plotted in Fig. 3. They are in good agreement with the results obtained from the fits of the images: $\Omega_{\rm eff} \simeq \Omega_{\rm stir}^{(2)}$. Consequently they conflict with the rotation frequency derived from the vortex surface density when $\Omega_{\rm stir}^{(2)}/2\pi = 66$–68 Hz.

To explain the absence of visible vortices in the regime $\Omega_{\rm stir}^{(2)}/2\pi = 66$–68 Hz, one could argue that the rotating gas might be relatively hot, hence described by classical physics. However all experiments shown here are performed in the presence of radio-frequency (rf) evaporative cooling. The rf is set 24 kHz above the value which empties the trap and it eliminates all atoms crossing the horizontal plane located at a distance $x_{\rm ev} \sim 19$ μm below the center (one-dimensional evaporation). From the evaporative cooling theory [35,36] we know that the equilibrium temperature T of the rotating gas is a fraction of the evaporation threshold $V_{\rm rot}(x_{\rm ev}) \sim 30$ nK for $\Omega_{\rm eff}/2\pi = 67$ Hz. This indicates that T is in the range of 5–15 nK, well below the critical temperature at this density (180 nK for an estimated density 3×10^{13} cm^{-3}) [37]. This low temperature is also confirmed by the small decay rates of the quadrupole modes (~ 20 s^{-1}), characteristic of $T \ll T_c$.

The estimated temperature T is of the order of μ, since the Thomas-Fermi law (3) gives $\mu = 8$ nK for $\Omega/(2\pi) = 67$ Hz. It is also similar to the splitting between Landau levels $2\hbar\omega_\perp/k_B = 6.3$ nK, so that only the first two or three levels are appreciably populated. For each Landau level, the rf evaporation eliminates states with an angular momentum $L_z/\hbar > (x_{\rm ev}/a_{\rm ho})^2 \sim 200$, where $a_{\rm ho} = \sqrt{\hbar/(m\omega_\perp)}$.

A first possibility to interpret our data consists in assuming that the gas shown in Figs. 1(e)–1(g) is rotating, that it is in the degenerate regime, but that it cannot be described by a single macroscopic wave function. A theoretical analysis along this line, involving the formation of composite bosons, has been proposed in [38]. We note however that such a fragmentation is usually expected when the number $N_{\rm lev}$ of single particle levels in an energy band of width μ is comparable with the atom number, while we have here $N_{\rm lev}/N \lesssim 10^{-2}$.

A second explanation is that the vortices are strongly tilted or bent for $\Omega \geq \omega_\perp$, so that they do not appear as clear density dips in the images of Figs. 1(e)–1(g). The distortion of the vortex lattice could result from (i) a strong increase of the crystallization time, (ii) a distortion due to the residual static anisotropy of the trap, or (iii) an increase of the fragility of the vortex lattice. To check for possibility (i), we increased τ_{eq} from 500 ms to 2 s without noticing any qualitative change in the atom distribution (for larger τ_{eq} the gas slows down significantly). Concerning option (ii), the Boulder group has shown for $\Omega = 0.95\,\omega_\perp$ that a static anisotropy of $\sim 4\%$ may reduce considerably the vortex visibility [33]. However the residual anisotropy of our trap is $<1\%$ and this effect should be limited. Finally if option (iii) is valid, the vortex lattice should be visible only at ultralow temperatures that cannot be reached in our experiment. A recent theoretical study [13,39] seems to favor this hypothesis: when looking for the ground state of the system using imaginary time evolution of the Gross-Pitaevskii equation, it was found that much longer times were required for $\Omega \gtrsim \omega_\perp$ to reach a well-ordered vortex lattice.

To summarize, we have presented in this Letter a direct evidence for a qualitative change in the appearance of a degenerate Bose gas, confined in a quadratic + quartic potential, when it is rotated around and just above the trapping frequency. The predicted existence of giant vortices in this type of potential [8–14] remains to be investigated. Another extension of the present work consists of transposing the experimental scheme to a 2D geometry, where the motion along z would be frozen. For $\Omega \sim \omega_\perp$ the situation would then be the bosonic analog of the situation leading to the quantum Hall effect.

We thank P. Rosenbusch for participation in earlier stages of this experiment and S. Stringari, L. Pitaevskii, G. Baym, and the ENS group for useful discussions. S. S. acknowledges support from the European Union (CQG network HPRN-CT-2000-00125), the Studienstiftung des deutschen Volkes, and the DAAD. This work is partially supported by CNRS, Collège de France, Région Ile de France, and DRED.

Note added.—Since the submission of this paper the Boulder group achieved a rapidly rotating Bose gas in the lowest Landau level [40].

*Unité de Recherche de l'Ecole normale supérieure et de l'Université Pierre et Marie Curie, associée au CNRS.

[1] R. J. Donnelly, *Quantized Vortices in Helium II* (Cambridge University Press, Cambridge, 1991), Chaps. 4 and 5.
[2] M. Tinkham, *Introduction to Superconductivity* (McGraw-Hill, New York, 1996).
[3] M. R. Matthews *et al.*, Phys. Rev. Lett. **83**, 2498 (1999).
[4] K.W. Madison, F. Chevy, W. Wohlleben, and J. Dalibard, Phys. Rev. Lett. **84**, 806 (2000).
[5] J. R. Abo-Shaeer, C. Raman, J. M. Vogels, and W. Ketterle, Science **292**, 476 (2001).
[6] E. Hodby *et al.*, Phys. Rev. Lett. **88**, 010405 (2002).
[7] P. C. Haljan, I. Coddington, P. Engels, and E. A. Cornell, Phys. Rev. Lett. **87**, 210403 (2001)
[8] A. L. Fetter, Phys. Rev. A **64**, 063608 (2001).
[9] E. Lundh, Phys. Rev. A **65**, 043604 (2002).
[10] K. Kasamatsu, M. Tsubota, and M. Ueda, Phys. Rev. A **66**, 053606 (2002).
[11] G. M. Kavoulakis and G. Baym, New J. Phys. **5**, 51.1 (2003).
[12] U. R. Fischer and G. Baym, Phys. Rev. Lett. **90**, 140402 (2003).
[13] A. Aftalion and I. Danaila, cond-mat/0309668.
[14] A. D. Jackson and G. M. Kavoulakis, cond-mat/0311066.
[15] J. Sinova, C. B. Hanna, and A. H. MacDonald, Phys. Rev. Lett. **89**, 030403 (2002).
[16] N. R. Cooper, N. K. Wilkin, and J. M. F. Gunn, Phys. Rev. Lett. **87**, 120405 (2001).
[17] B. Paredes, P. Fedichev, J. I. Cirac, and P. Zoller, Phys. Rev. Lett. **87**, 010402 (2001).
[18] T.-L. Ho, Phys. Rev. Lett. **87**, 060403 (2001).
[19] N. Regnault and Th. Jolicœur, Phys. Rev. Lett. **91**, 030402 (2003).
[20] U. R. Fischer, P. O. Fedichev, and A. Recati, cond-mat/0212419.
[21] C. Raman, J. R. Abo-Shaeer, J. M. Vogels, K. Xu, and W. Ketterle, Phys. Rev. Lett. **87**, 210402 (2001).
[22] P. Rosenbusch *et al.*, Phys. Rev. Lett. **88**, 250403 (2001).
[23] P. Engels, I. Coddington, P. C. Haljan, V. Schweikhard, and E. A. Cornell, Phys. Rev. Lett. **90**, 170405 (2003).
[24] S. Stock, V. Bretin, F. Chevy, and J. Dalibard, cond-mat/0311099.
[25] K.W. Madison, F. Chevy, V. Bretin, and J. Dalibard, Phys. Rev. Lett. **86**, 4443 (2001).
[26] F. Zambelli and S. Stringari, Phys. Rev. Lett. **81**, 1754 (1998); M. Cozzini and S. Stringari, Phys. Rev. A **67**, 041602(R) (2003).
[27] P. Rosenbusch, V. Bretin, and J. Dalibard, Phys. Rev. Lett. **89**, 200403 (2002).
[28] Y. Castin and R. Dum, Phys. Rev. Lett. **77**, 5315 (1996).
[29] E. Lundh, C. J. Pethick, and H. Smith, Phys. Rev. A **58**, 4816 (1998).
[30] Y. Castin and R. Dum, Eur. Phys. J. D **7**, 399 (1999).
[31] Such a simple formula could not be obtained for the column density along y, hence the absence of a fitting function in Fig. 2(b).
[32] This value for Ω_{eff} is systematically slightly below the one derived from the cloud's radius as also found in [21].
[33] P. Engels, I. Coddington, P. C. Haljan, and E. A. Cornell, Phys. Rev. Lett. **89**, 100403 (2002).
[34] F. Chevy, K.W. Madison, and J. Dalibard, Phys. Rev. Lett. **85**, 2223 (2000).
[35] W. Ketterle and N. Van Druten, Adv. At. Mol. Opt. Phys. **37**, 181 (1996).
[36] O. Luiten, M. Reynolds, and J. Walraven, Phys. Rev. A **53**, 381 (1996).
[37] The rotation of the gas is crucial for establishing a link between the evaporation radius and the temperature. For a gas at rest, the evaporation threshold is $V(x_{ev})$ instead of $V_{rot}(x_{ev})$, which corresponds to a much higher temperature (100–200 nK).
[38] E. Akkermans and S. Ghosh, cond-mat/0307418.
[39] A. Aftalion and I. Danaila (private communication).
[40] V. Schweikhard *et al.*, Phys. Rev. Lett. **92**, 040404 (2004).